Failure analysis of brittle elastic notched structures utilising finite fracture mechanics procedures

Jochen Hebel[1, a], Wilfried Becker[1, b],

Dominique Leguillon[2, c] and Zohar Yosibash[3, d]

[1]Technische Universität Darmstadt, Fachgebiet Strukturmechanik,
Hochschulstraße 1, 64289 Darmstadt, Germany

[2]LMM-CNRS UMR 7607, Université Pierre et Marie Curie, 75252 Paris Cedex 05, France

[3]Pearlstone Center for Aeronautical Engineering Studies, Department of Mechanical Engineering,
Ben-Gurion University of the Negev, Beer-Sheeva 84105, Israel

[a]hebel@mechanik.tu-darmstadt.de, [b]becker@mechanik.tu-darmstadt.de,
[c]dol@ccr.jussieu.fr, [d]zohary@bgu.ac.il

Keywords: Brittle fracture, finite fracture mechanics, failure initiation, notch, mixed-mode.

Abstract. In this study, different types of finite fracture mechanics procedures to predict crack initiation in brittle elastic notched structures subject to mixed-mode loading are investigated. A hybrid failure model is employed taking into account the stress field in the undamaged structure and the energy balance for the formation of cracks exhibiting a finite length. Asymptotic formulations are compared to a direct numerical implementation. Experiments carried out on notched brittle specimens exhibiting various geometries and loading-modes are analysed by means of both approaches. It is found that the predictions from the model agree well with the experimental results. Furthermore, the dominance of the asymptotical formulations for finite geometries is discussed.

Introduction

Due to its relevance to many applications, numerous models have been formulated to describe brittle failure initiation. Special efforts have been made to account for theoretically singular problems occurring at geometrical and material discontinuities as well as for different kinds of size effects. Proposed approaches include local and non-local evaluations of field quantities such as stress and strain energy density. Additionally, specific geometry-dependent parameters have been suggested. In general, more than one material parameter is required for an adequate description.

The hybrid failure criterion [1] as applied in this study employs a strict simultaneous consideration of strength and toughness criteria utilising a finite fracture mechanics [2, 3] approach. Its formulation has the advantage of generally covering the extreme cases of homogeneous stress fields and existing cracks as well as any intermediate stress concentration.

Regarding its implementation, efficient asymptotical formulations [1, 4-6] requiring solely an analysis of the undamaged structure have been formulated. However, the dominance requirements for the asymptotic fields pose restrictions on the structure and the analysed load case. Alternatively, direct numerical models have been suggested for interface problems [7, 8] as well as for the general case of straight cracks emanating from an investigated point [9, 10]. They do not exhibit such severe restrictions. On the other hand, they require high computational effort as failure load and mode need to be determined in an iterative manner. In this study, both approaches are compared on the basis of experimental results carried out on notched PMMA specimens subject to mixed-mode-loading. Furthermore, the dominance limits of the asymptotic analyses are investigated.

Hybrid failure criterion

Fundamental to the hybrid failure model [1] is the spontaneous formation of a crack having a finite area ΔA if a stress criterion $F(\sigma_{ij})$ is fulfilled over the full area and if the incremental energy release rate $\bar{\mathcal{G}}$ reaches the fracture resistance of the material:

$$F\left(\sigma_{ij}\right) \geq \sigma_c \wedge \bar{\mathcal{G}} = -\frac{\Delta\Pi}{\Delta A} = \mathcal{G}_c, \tag{1}$$

where $\Delta\Pi$ denotes the change in potential energy due to crack formation. Utilising the fundamental material parameters strength σ_c and toughness $\mathcal{G}_c$, it is applicable to a wide range of problems. For the stress criterion of Eq. 1, depending on the material, an appropriate function $F(\sigma_{ij})$ is chosen, e. g. the maximum principal stress

$$\sigma_I \geq \sigma_c \tag{2}$$

or the maximum circumferential stress acting perpendicular to the newly created crack face

$$\sigma_{\varphi\varphi} \geq \sigma_c. \tag{3}$$

Alternatively, a stress criterion of the type

$$\frac{1}{\Delta a} \int_0^{\Delta a} \sigma_{\varphi\varphi}\left(r\right) \mathrm{d}r = \sigma_c \tag{3}$$

has been suggested [11]. Regarding the crack geometry, in general all kinematical admissible displacement fields should be considered, although the sole consideration of a straight crack is sufficient in many cases.

Asymptotic formulations

Asymptotic expansions of the stress field and the incremental energy release rate provide efficient means of evaluating the hybrid failure criterion from a single analysis of the undamaged structure for many problem classes. Subsequently, two formulations for isotropic linear-elastic problems as used for the following analyses are presented.

Sharp V-notch. An infinite domain with a crack emanating from a V-notch [4] is considered for traction–free notch and crack faces. At infinity, the leading terms of the asymptotic expansion in isotropic linear elasticity for the domain without crack are applied with displacements

Fig. 1: V-notch with emanating crack.

$$u_i\left(r,\varphi\right) = u_{i0} + A_1 r^{\alpha_1} \hat{f}_i^{(1)}\left(\varphi\right) + A_2 r^{\alpha_2} \hat{f}_i^{(2)}\left(\varphi\right) + \cdots \tag{4}$$

and stresses

$$\sigma_{ij}\left(r,\varphi\right) = A_1 r^{\alpha_1-1} \tilde{f}_{ij}^{(1)}\left(\varphi\right) + A_2 r^{\alpha_2-1} \tilde{f}_{ij}^{(2)}\left(\varphi\right) + \cdots. \tag{5}$$

The exponents α_1 and α_2 as well as the circumferential distributions $\tilde{f}_{ij}^{(k)}\left(\varphi\right)$ solely depend on the notch angle ω and are calculated from a corresponding eigenvalue problem. The circumferential

17th European Conference on Fracture
2-5 September, 2008, Brno, Czech Republic

ECF17
ECF17

BRNO '08
IX 2 - 5
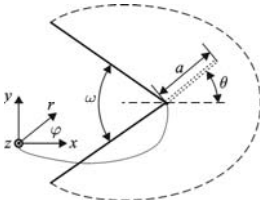
distributions $\hat{f}_i^{(k)}(\varphi)$ depend on the elastic constants as well. Loading mode and intensity are characterised by the generalised stress intensity factors for symmetric (A_1) and antisymmetric (A_2) contributions. As a prerequisite for asymptotical investigations, the ratio A_2/A_1 has to be determined from a complete analysis of the undamaged structure. The incremental energy release $-\Delta\Pi = -\left(\Pi(a) - \Pi(a=0)\right)$ is also expressed by an asymptotic expansion

$$-\Delta\Pi(a,\theta) = A_1^2 a^{2\alpha_1} H_{11}(\omega,\theta) + A_1 A_2 a^{\alpha_1+\alpha_2}\left(H_{12}(\omega,\theta) + H_{21}(\omega,\theta)\right) + A_2^2 a^{2\alpha_2} H_{22}(\omega,\theta) + \cdots, \qquad (6)$$

where a and θ denote length and orientation of the newly created crack. The functions $H_{ij}(\omega,\theta)$ also depend on the elastic constants and are calculated numerically from a boundary layer analysis with Dirichlet boundary conditions from Eq. 4 applied in the far field.

Circular hole. Similarly, an asymptotic solution for the case of a plate with a circular hole [12, 9, 5] subject to uniaxial tension can be constructed straightforwardly. The circumferential stress $\sigma_{\varphi\varphi}(r,\varphi)$ for an infinite plate is given by the equation
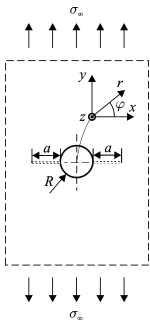
$$\sigma_{\varphi\varphi}(r,\varphi) = \frac{\sigma_\infty}{2}\left[1 + \frac{R^2}{r^2} + \left(1 + 3\frac{R^4}{r^4}\right)\cos 2\varphi\right]. \qquad (7)$$

For a homogeneous symmetrical isotropic configuration, it can be expected, that two cracks will emanate in horizontal direction at the locations $\varphi = 0$ and $\varphi = \pi$ where $\sigma_{\varphi\varphi}$ exhibits a maximum. For plane strain, the incremental energy release rate $\bar{\mathcal{G}}(a)$ is calculated from the stress intensity factor yielding

Fig. 2: Circular hole with emanating cracks.

$$\bar{\mathcal{G}}(a) = (1-\upsilon^2)\frac{\sigma_\infty^2 \pi}{aE}\int_R^{R+a} F^2\left(\frac{r}{R}\right) r\,\mathrm{d}r, \qquad (8)$$

where F is a tabulated function (see e.g. [13]).

Direct numerical formulation
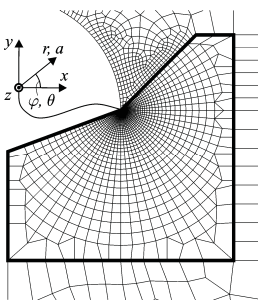
In order to apply the criterion to a wider class of problems, direct numerical formulations have been suggested [7-10]. For plane problems, the model is discretised by means of straight cracks emanating from one point. A universally applicable analysis procedure as depicted in Fig. 3 to be used within a finite element (FE) program has been implemented for the application of the above criterion to structural problems. It includes automated pre- and postprocessing for the uncracked configuration as well as for a configuration with a straight crack of given length a and direction θ starting at the investigated point. The stress criterion $F(\sigma_{ij}(r,\varphi))$ is evaluated for the uncracked geometry and for the cracks , the incremental energy release rates $\bar{\mathcal{G}}$

Fig. 3: FE analysis model.

are computed:

$$\bar{\mathcal{G}}(a,\theta) = -\frac{\Delta\Pi^I}{\Delta a} - \frac{\Delta\Pi^{II}}{\Delta a} = \bar{\mathcal{G}}^I + \bar{\mathcal{G}}^{II} = \frac{1}{\Delta a}\int_0^{\Delta a}\mathcal{G}^I\,\mathrm{d}a + \frac{1}{\Delta a}\int_0^{\Delta a}\mathcal{G}^{II}\,\mathrm{d}a. \qquad (9)$$

In linear elasticity, the potential differences can be calculated efficiently by means of discretised crack closure integrals.

Computation of the failure load

In general, the evaluation of the failure model (Eq. 1) at a given point poses a nonlinear optimisation problem for the failure load, independent of the model formulation. Solely the computational cost for the calculations will differ between asymptotical and direct numerical formulation. Subsequently, the load is described by a scalar parameter P, whereas for combined load cases an appropriate vectorial formulation will be necessary. The failure load P_f is the load at which crack of length a_f and the orientation θ_f will be initiated in the sector $\theta_l \le \theta \le \theta_u$:

$$P_f = \underset{P>0,\, a>0,\, \theta_l \le \theta \le \theta_u}{\text{Min}} \left\{ P \,|\, \bar{\mathcal{G}}(P,a,\theta) = \mathcal{G}_c,\, F(P,a,\theta) \ge \sigma_c \right\}. \tag{10}$$

In close proximity to sufficiently strong stress concentrations, it can be assumed that

$$\frac{\partial \bar{\mathcal{G}}}{\partial a} > 0 \ \forall \ a \le a_f. \tag{11}$$

If additionally, with respect to the stress criterion, the conditions

$$F(\sigma_{ij}) \ge \sigma_c \ \forall \ a \le a_f, \tag{12}$$

and

$$\left. \frac{\partial F}{\partial a} \right|_{a=a_f} < 0, \tag{13}$$

hold, $P_{f\varphi}$ is obtained as the solution of the unconstrained optimisation problem

$$\underset{P>0}{\text{Min}} \left\{ \left[\bar{\mathcal{G}}(P, a_c(P,\theta), \theta) - \mathcal{G}_c \right]^2 \right\} \tag{14}$$

for a given angle θ. The contour around the investigated point on which the stress criterion is exactly fulfilled is denoted as a_c. For the asymptotical submodels, the conditions in Eqs 11-13 hold automatically but need to be checked in the numerical procedure. The minimum value obtained for $P_{f\theta}(\theta)$ yields the failure load P_f. Standard optimisation procedures are used for the iterative solution of the problems.

Analysis of experimental results

Table 1: Material data for PMMA.

Ref.	E [MPA]	ν [-]	σ_c [MPa]	$\mathcal{G}_c$ [J/m^2]
[4]	3100	0.36	111.8	368.3 ±70.4
[14]	3300	0.35	102.8	384.2
[12]	3000	0.36	72.0	290.0

Three reported data sets from experiments carried out on PMMA specimens are analysed using the different formulations. Reported material data as used for the analysis are given in Table 1.

V-notched specimens subject to asymmetric bending [4, 15]. Three-point bending experiments on V-notched specimens exhibiting a thickness of 10 mm have been carried out. Asymmetric loading and support configurations as depicted in Fig. 4a lead to mixed-mode-loading. For this data set with spatially fixed bearings and load application point, a mode mixity parameter m_b is introduced:
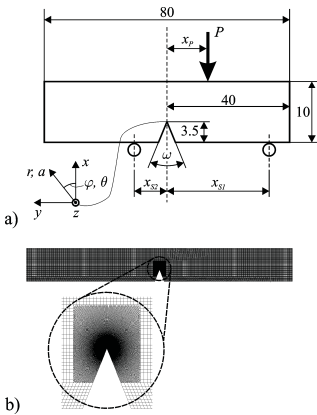
$$m_b = \begin{cases} 0 \text{ for } x_P = 0, \\ \dfrac{2}{\pi}\arctan\left(\dfrac{10 \text{ mm}}{l - 2x_P}\right) \text{ for } 0 < x_P < \dfrac{x_{S1} + x_{S2}}{2}, \end{cases} \quad (15)$$

From the ratio of shear and normal stresses for the simply supported beam, it characterizes symmetric and antisymmetric contributions similarly to the parameter m_t for inclined tension (Eq. 16).

The asymptotic analysis [4] has been carried out utilising a p-FE-model, from which the generalised stress intensity factors have been extracted. In Fig. 4b, the standard plane strain FE-model (290,000 DOF) as used for the direct numerical approach is shown. In the finely meshed area around the notch root, crack initiation is investigated for initial crack lengths ranging from 0.001 mm-2.0 mm with an angular increment of 0.75°. Results from both approaches are compared in Fig. 5.

Fig. 4: V-notched bending specimens: Experimental set-up (dimensions in mm) (a), FE model (b).
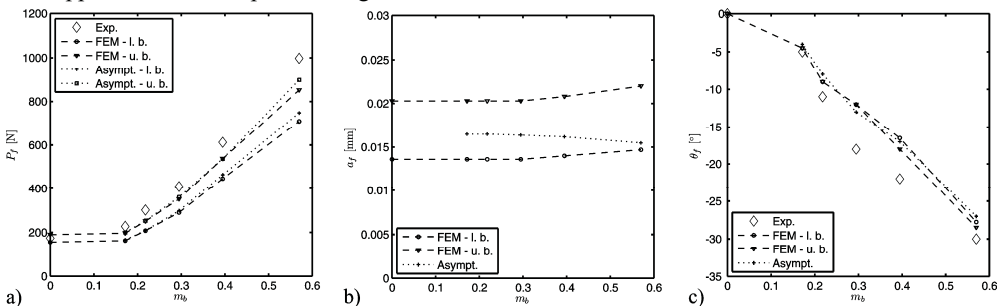
Fig. 5: V-notched bending specimens: Failure loads (a), crack initiation lengths (b), crack initiation angles (c).

Regarding the predicted failure load P_f, both approaches underestimate the experimental results. An increasing deviation is observed for increasing mode mixity ratios. Asymptotical and direct numerical approach agree well. The crack initiation length a_f is almost constant. A significant influence of the higher and lower bound values for the fracture toughness on the crack initiation length is shown by the direct numerical approach, whereas an insignificant influence is observed on the crack initiation angle. In general, the initiation angle θ_f is predicted well with an increasing deviation between simulation and experiment for increasing mode mixity ratios.

Inclined V-notched specimens subject to tension [14]. Secondly, reported tension experiments on as depicted in Fig 6a have been investigated. The specimens of a thickness of 5 mm are rotated about the angle ψ leading to an increasing mode mixity characterised by the parameter

$$m_t = \psi \frac{2}{\pi}. \quad (16)$$
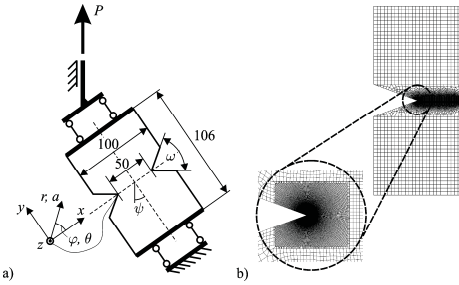
Fig. 6: Inclined V-notched tension specimens: Experimental set-up (dimensions in mm) (a), FE model (b).

Again, a p-FEM-procedure has been used for the asymptotic analysis [4]. In Fig. 6b, the plane strain FE-model (155,000 DOF) for the direct approach is depicted. Due to the point-symmetry of the problem with respect to the centre in the cracked as well as in the uncracked state, a half-model with appropriate point symmetry conditions is sufficient. A comparison of the results for a notch angle of $\omega = 40°$ is shown in Fig. 7. The failure load P_f is predicted well by both asymptotic and direct numerical approach. Different tendencies for the crack initiation length a_f are observed. Similar to the previous example but much more pronounced, a decrease in the crack initiation length predicted by the asymptotical approach is observed, whereas an increase is predicted by the direct numerical approach with increasing differences for increasing mode mixity ratios. Both procedures yield an accurate prediction of the initiation angle θ_f up to high mode mixity ratios.
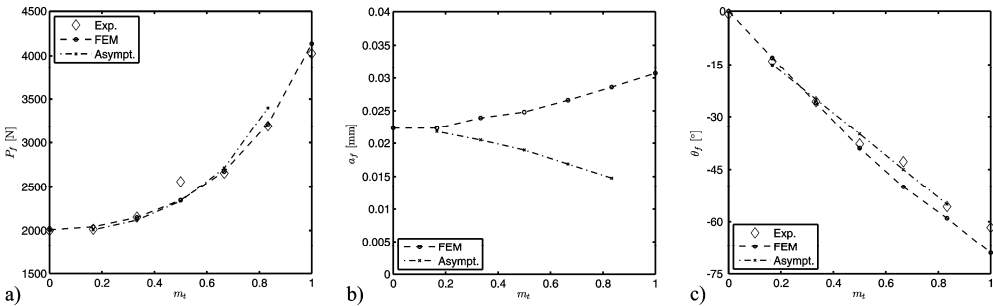
Fig. 7: Inclined V-notched tension specimens ($\omega = 40°$): Failure loads (a), crack initiation lengths (b), crack initiation angles (c).

For notch angles of $\omega = 80°$, the results are shown in Fig. 8. The deviation between experiment and theory for failure load P_f and crack initiation angle θ_f is higher in absolute terms. Asymptotical and direct numerical approach agree well . Even for the crack initiation length a_f, similar tendencies are reported for both approaches.
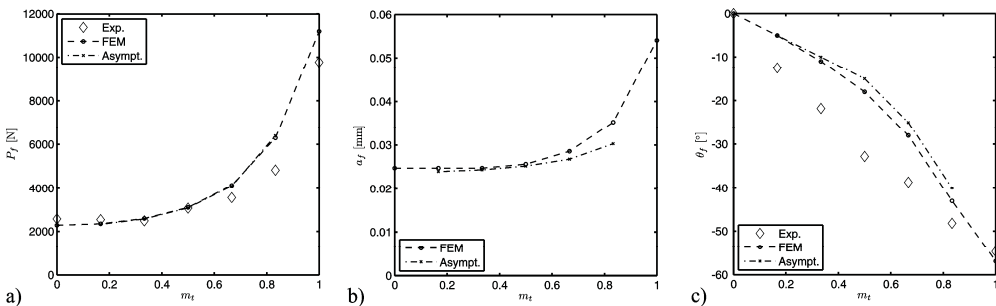
Fig. 8: Inclined V-notched tension specimens ($\omega = 80°$): Failure loads (a), crack initiation lengths (b), crack initiation angles (c).

Specimens with circular holes subject to tension [12].
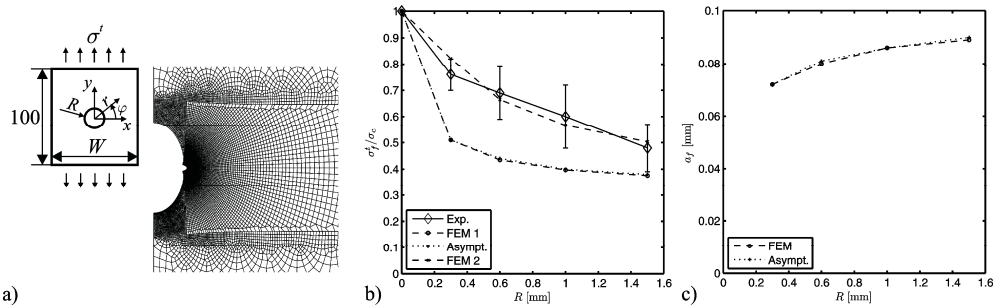
Fig. 9: Tension specimens with circular holes: Experimental set-up (dimensions in mm) and FE model (a), failure loads (b), crack initiation lengths (c).

Size effects have been investigated for specimens with circular holes and a thickness of 5 mm subject to uniaxial tension. Experimental set-up and FE model are shown Fig. 9a, analysis results for $W = 30$ mm in Fig. 9b and c. Both analytical and direct numerical procedure yield similar results for the failure load σ_{tf} / σ_c as well as for the length a_f of the initiated crack. However, if the given fracture toughness values are used, the failure load σ_{tf} / σ_c is severely underestimated by the model (**FEM 1**). Using the given strength σ_c and recalculating $\mathcal{G}_c$ from the experiments yields an average value of $\mathcal{G}_c = 1472$ N/mm. Calculations using this toughness denoted as **FEM 2** show good coverage of the size effect. Although, as shown in Table 1, the fracture toughness values show a wide scatter, this value is well beyond. Therefore, additional toughening effects not covered by the model can be expected to prevail.

Dominance analysis for asymptotic expansions

For all investigated configurations, general agreement between both approaches has been found, indicating dominance of the asymptotic submodels. In engineering practice, this will not always be the case when the stress concentration is not small compared to the rest of the structure. This case is investigated in the following section for modified tension specimens with circular holes ($R = 0.6$ mm), for which $2R/W$ is varied.

Failure loads σ_{tf} / σ_c and crack initiation lengths a_f are compared in Fig. 10. In the recalculated experimental results, the most extreme case investigated exhibited an ratio $2R/W = 0.1$, for which the deviation between asymptotic and numerical solution is comparably small. For increasing ratios, an increasing deviation is observed, which is more pronounced for the failure load than for the crack initiation length. For all investigated cases, a crack initiation angle of $\theta_f = 0°$ is predicted by the direct numerical model which may not be the case for extremely high ratios $2R/W$.

In Fig. 11, the asymptotic solution (Eq. 7) is compared to the numerical solution for both states. The relative deviation $\bar{\mathcal{E}}^{as}(x - R)$ of the asymptotic
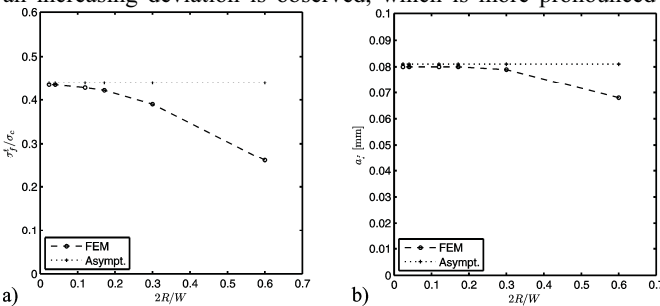
Fig. 10: Tension specimens with holes, Variation of W for $R = 0.6$ mm: Failure loads (a), crack initiation lengths (b).
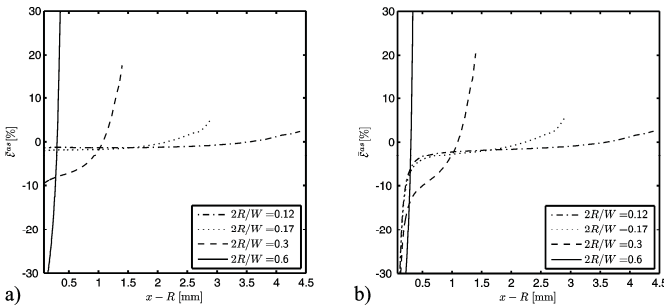
Fig. 11: Tension specimens with circular holes, Variation of W for $R = 0.6$ mm, relative deviation of asymptotic solution of $\sigma_{\varphi\varphi}(x)$: Uncracked (a) and cracked (b) state.

solution is plotted over the distance from the hole boundary.

For the uncracked state, a domain of validity is observed for $2R/W \leq 0.17$, corresponding well with the results for the failure loads. Although a strong deviation in close proximity to the crack tip is observed for the cracked state, a similar domain of validity exists in the far field. The stresses are underestimated leading to the overrated failure load. As long as the length of the initiated crack is small with respect to the investigated structure, asymptotic approaches appear to be applicable as long as the stress field in the uncracked state is approximated well by the asymptotic solution.

Conclusions

Asymptotical and direct numerical finite fracture mechanics procedures have been compared in this study. For the investigated specimen geometries, good agreement was found between experiment and theory as well as between both procedures. However, in engineering practice, the dominance of the asymptotic fields may not prevail as shown for modified geometries. Though being numerically less efficient, the direct approach provides a reliable solution for these cases.

References

[1] D. Leguillon: Eur. J. Mech. A/Solids Vol. 21 (2002), pp. 61-72.

[2] Z. Hashin: J. Mech. Phys. Solids Vol. 44 (1996), pp. 1129-1145.

[3] D. Taylor et al.: Eng. Fracture Mech. Vol. 72 (2005), pp. 1021-1038.

[4] Z. Yosibash et al.: Int. J. Fracture Vol. 141 (2006), pp. 291-312.

[5] D. Leguillon et al.: Eng. Fracture Mech. Vol. 74 (2007), pp. 2420-2436.

[6] C. Henninger and D. Leguillon: J. Thermal Stresses Vol. 31 (2008), pp.59-76.

[7] A. Müller et al.: Proc Appl. Math. Mech. Vol. 4 (2004), pp. 288-289.

[8] A. Müller et al.: Eng. Fracture Mech. Vol. 73 (2006), pp. 994-1008.

[9] J. Hebel and W. Becker: Proc Appl. Math. Mech. Vol. 6 (2006), pp. 169-170.

[10] J. Hebel and W. Becker: Mech. Adv. Mater. Struct., accepted for publication.

[11] P. Cornetti et al.: Eng. Fracture Mech. Vol. 73 (2006), pp. 2021-2033.

[12] J. Li and X. B. Zhang: Eng. Fracture Mech. Vol. 73 (2006), pp. 505-523.

[13] Y. Murakami (ed.): *Stress intensity factors handbook* (Pergamon Press 1987).

[14] A. Seweryn et al.: J. Eng. Mech. ASCE, Vol. 123 (1997), pp. 535-543.

[15] E. Priel et al.: Int. J. Fracture Vol. 144 (2007), pp. 247-265.